DOI: 10.1021/cg9009724

CRYSTAL GROWTH & DESIGN
Communication
2009, Vol. 9
4602–4606

Synthesis and Wavelength-Tunable Luminescence Property of Wurtzite $Zn_xCd_{1-x}S$ Nanostructures

Changqing Jin,[†] Wei Zhong,*[,†] Xin Zhang,[†] Yu Deng,[†] Chaktong Au,[‡] and Youwei Du[†]

[†]*Nanjing National Laboratory of Microstructures and Department of Physics, Nanjing University, Nanjing 210093, People's Republic of China, and* [‡]*Chemistry Department, Hong Kong Baptist University, Hong Kong, People's Republic of China*

Received August 14, 2009; Revised Manuscript Received September 15, 2009

ABSTRACT: High-quality nanostructured $Zn_xCd_{1-x}S$ has been synthesized through a method of two-step thermal evaporation. The typical morphologies of the nanomaterials were investigated by SEM and TEM. The first step of synthesis is the preparation of ZnS nanoribbons. With ZnS nanoribbons being used as templates, a series of wurtzite $Zn_xCd_{1-x}S$ ($x = 0.47$, 0.70, 0.77, 0.85, and 0.94) nanobelts can be produced. Furthermore, by adopting ZnS nanoribbons of a particular width, $Zn_xCd_{1-x}S$ nanobelts of a desired width can be fabricated. In XRD analysis, we find that with an increase in Zn content (x), the peaks corresponding to the wurtzite structures shift to larger 2θ. As a deduction based on Vegard's law, the $Zn_xCd_{1-x}S$ are solid solutions of similar crystal structure. The results of HRTEM and SAED investigations reveal that the ZnS nanoribbons and $Zn_xCd_{1-x}S$ nanobelts grow along the $\langle 10\bar{1}0\rangle$ direction. With an increase in Zn content, we observe a gradual blue shift of photoluminescence emission (from 443 to 352 nm), further indicating the homogeneity of the $Zn_xCd_{1-x}S$ solid solutions. After proper thermal annealing, there is better crystallinity of $Zn_xCd_{1-x}S$ and higher specificity of near-band emission.

One-dimensional (1D) nanostructures (such as nanotubes, nanowires and nanobelts) that are tunable in size, morphology, and crystallographic orientation are of particular interest in nanotechnology. The nanomaterials show functionalities potentially applicable in a wide range of industries.[1−8] ZnS, a direct gap compound of II−VI group with room-temperature (RT) band gap energy of 3.7 eV, is one of the first semiconductors discovered and probably one of the most important materials in the electric and optoelectronic industries. In the past decade, various 1D ZnS nanostructures were synthesized through multifarious methods.[9−11] Among them, ZnS nanobelts are binary semiconductors with properties potentially apt for optical and electronic applications.[13−15] Indeed, single-crystalline ZnS nanobelts were synthesized by Fang et al. as ultraviolet-light sensors and field emitters.[16] For semiconductors, band gap energy is an important parameter that determines electronic and optical properties. Because of the discrete band gaps of binary semiconducting materials, they are limited in applications. The ternary semiconductor materials (such as $Zn_xCd_{1-x}S$) are successive in band gap energy. A successful fabrication of ZnS-based ternary semiconductors with band gaps ranging from 2.4 to 3.7 eV would substantially widen the prospect of application. To the best of our knowledge, although ZnCdS films and $Zn_xCd_{1-x}S$ nanoparticles were prepared by various methods,[12,18,24,25] the synthesis of 1D ZnCdS nanostructures through a method of two-step thermal evaporation has not been reported before.

Herein, we report the synthesis of wurtzite $Zn_xCd_{1-x}S$ nanobelts (in high yield) through a method of two-step thermal evaporation. A quartz tube with an inner diameter of 48 mm and length of 800 mm was installed in a tube furnace. Then a ceramic boat loaded with zinc sulfide powder was placed in the center of the furnace. A piece of Si(111) substrate with the exposed surface coated with Au (7.5−30 nm thick) was placed in a ceramic boat located downstream (approximately 80 mm from the center of the source). After evacuation to a base pressure of ca. 1×10^{-3} Pa, the system was purged with high-purity Ar (used as carrier gas as well) at a flow rate of 20 sccm (standard cubic centimeters per minute). The ZnS powder was heated to 850 °C in a span of 1.5 h, and kept at this temperature for 1 h. In the meantime, the temperature of the Si(111) substrate was maintained at about 650 °C. After the deposition of materials on the substrate, the whole system was cooled to RT and the Ar supply was disconnected. The as-obtained product was the ZnS nanoribbons. Then cadmium sulfide powder was placed in the center of the furnace where the zinc sulfide powder was placed. At a pressure of ca. 1×10^{-3} Pa, CdS powder was evaporated at 950 °C for 1 h. Using Ar as carrier gas and ZnS nanoribbons as template, $Zn_xCd_{1-x}S$ was formed on the Si(111) substrate (maintained at about 700 °C). Finally, the as-synthesized product was annealed at 600 °C for 3 h under the protection of Ar (atmospheric pressure)

We found that the yield of product was high, and the generation of the nanobelts reproducible. The crystal structure of the products was determined by X-ray diffraction (XRD, D/Max-RA, Rigaku, Japan, Cu $K\alpha$). As shown in Figure 1, the diffraction peaks can be indexed to the wurtzite phase, indicating the formation of $Zn_xCd_{1-x}S$ crystallites. For our $Zn_xCd_{1-x}S$ system, x can be ascertained by the Vegard's law: $C_x = C_{CdS} + (C_{ZnS} - C_{CdS})x$ (where C_{ZnS}, C_{CdS}, and C_x are lattice constants along the c-axis of ZnS, CdS, and $Zn_xCd_{1-x}S$ crystals, respectively), in good agreement with the experimental results of $Zn_xCd_{1-x}S$ solid solutions and thin films.[17−19] In the calculation of x, we used the diffraction peaks of the (002) and (101) planes, which are at $2\theta = 28.501°$ and $2\theta = 30.528°$, respectively, for ZnS (the Joint Committee on Powder Diffraction standards (JCPDS) card No. 36-1450) and at $2\theta = 26.535°$ and $2\theta = 28.216°$ for CdS (JCPDS card No. 77-2306). From Figure 1, one can see that with an increase in Zn contents, there is a gradual decrease in lattice spacing along the c-axis (from 6.52, 6.41, 6.34, to 6.30 Å). The results confirm the formation of $Zn_xCd_{1-x}S$ solid solutions of similar crystallinity.

Shown in Figures 2 and 3 are the morphologies of the ZnS materials as observed by scanning electron microscopy (SEM). At a ZnS at-source temperature of 850 °C and an initial ZnS quantity of 0.097 g, uniform ZnS nanoribbons up to one millimeter in length were formed (Figure 2a). At high magnification (Figure 2b), one can see that the surfaces of the nanoribbons are smooth, and the width is about 400 nm. It is worth pointing out that some of the nanoribbons show a side edge that is sawlike.

*Corresponding author. E-mail: wzhong@nju.edu.cn. Fax: +86-25-83595535. Tel: +86-25-83621200.

 Published on Web 09/23/2009

Figure 3 shows the SEM images of ZnS nanoribbons generated at a ZnS at-source temperature of 950 °C and an initial ZnS quantity of 0.970 g. In this case, the nanoribbons are hundreds of micrometers in length and about 4000 nm in width. In other words, the width of the ZnS nanoribbons is highly dependent on the at-source temperature and the quantity of ZnS. Because a higher at-source temperature and a larger quantity of ZnS would mean a high concentration of ZnS vapor, broader ZnS nanoribbons are generated.

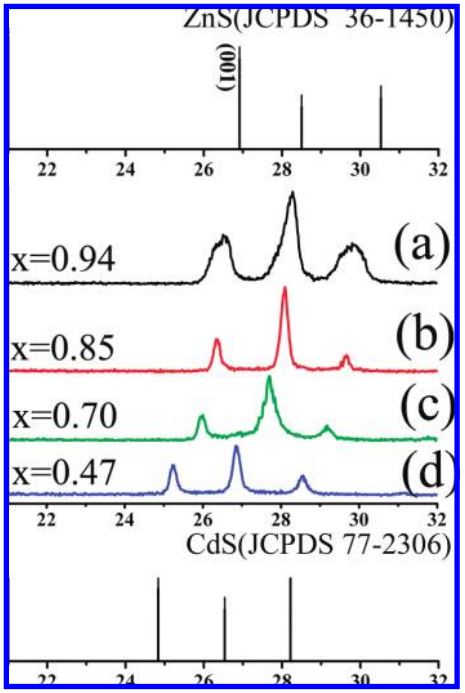

Figure 1. XRD patterns of $Zn_xCd_{1-x}S$ nanobeltss.

Shown in Figure 4 is the morphology of $Zn_xCd_{1-x}S$ nanosturctures fabricated using ZnS nanoribbons with width of about 400 nm as template. The $Zn_xCd_{1-x}S$ nanobelts are 60−100 nm in thickness, 300−600 nm in width and several hundreds of micrometres in length. Also, one can see rough edges along the sides of the nanobelts. The inset of Figure 4b is the energy-dispersive X-ray (EDX) spectrum of the sample that confirms the presence of Zn, Cd, and S elements. The x value estimated based on the EDX results is 0.85, consistent with that obtained in XRD investigation. Figure 4c shows the $Zn_xCd_{1-x}S$ nanobelts fabricated using ZnS nanoribbons with width of 1.5−3 μm as template. In this case, the $Zn_xCd_{1-x}S$ belts are with widths of about 2.5 μm. In Figure 4d, one can see rough edges of $Zn_xCd_{1-x}S$ nanobelts that are teethlike.

The transmission electron microscopy (TEM) and high-resolution TEM (HRTEM) images of ZnS nanoribbons are exhibited in Figure 5. Figure 5a shows the TEM bright-field image and selected area electron diffraction (SAED) pattern of a single ZnS nanoribbon, displaying width of ca. 400 nm and thickness of ca. 70 nm. The SAED pattern suggests single crystallinity, and the spots can be indexed to a wurtzite structure with lattice parameters of $a = 3.83$ Å and $c = 6.26$ Å. The corresponding HRTEM image (Figure 5b) further confirms the high single-crystallinity of the nanoribbon, showing 3.31 Å and 6.26 Å lattice spacing of $(10\bar{1}0)$ and (0001) planes, respectively. The SAED and HRTEM results suggest that the growth of the ZnS nanoribbon is along the $\langle 10\bar{1}0 \rangle$ direction. The results of our experiments also show that the ZnS nanoribbon with a sawlike edge is single-crystalline and grows along the $\langle 0001 \rangle$ direction. The deduction is that the ZnS

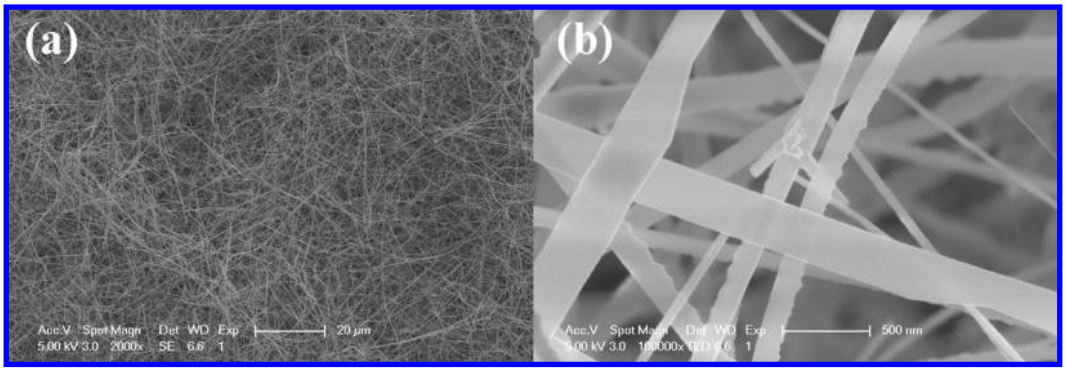

Figure 2. FE-SEM images of ZnS nanoribbons prepared at a ZnS at-source temperature of 850 °C and an initial ZnS at-source quantity of 0.097 g: (a) low and (b) high magnification.

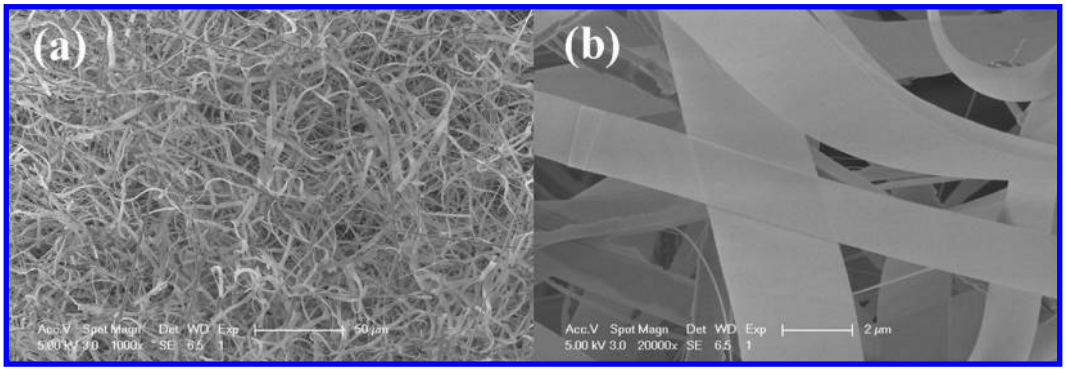

Figure 3. FE-SEM images of ZnS nanoribbon prepared at a ZnS at-source temperature of 950 °C and an initial ZnS at-source quantity of 0.97 g: (a) low and (b) high magnification.

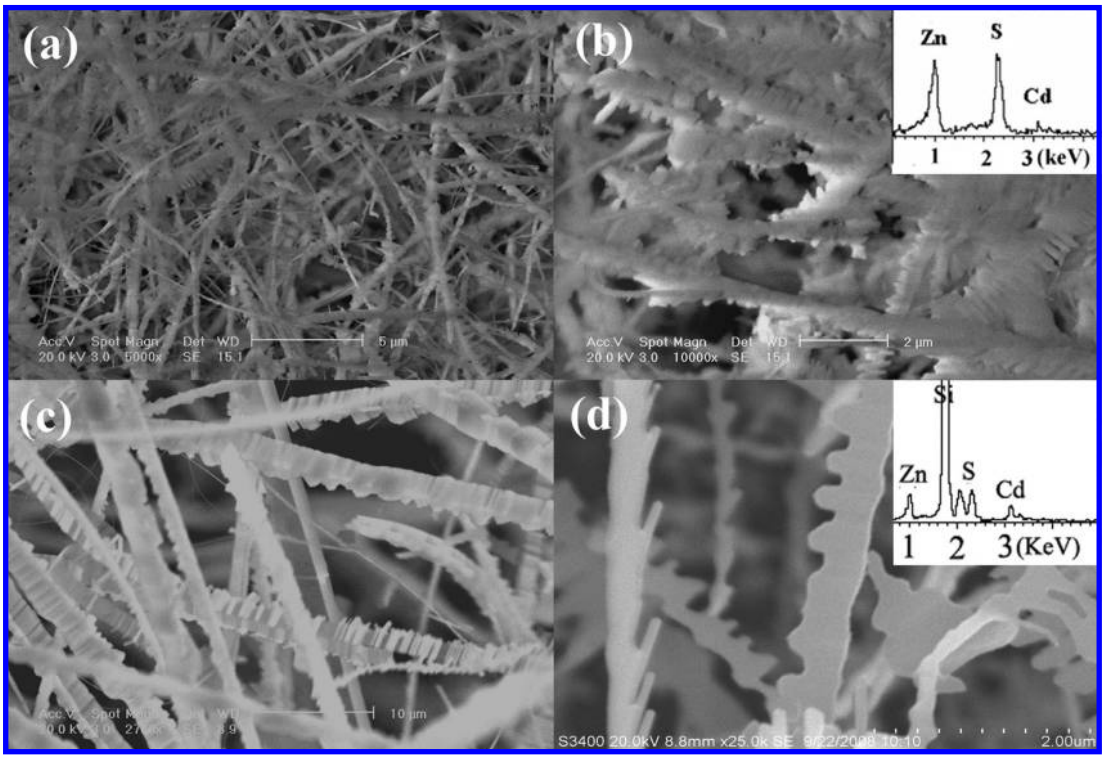

Figure 4. SEM images of $Zn_xCd_{1-x}S$ nanobelts at different magnifications (inset, EDX results), (b) $Zn_{0.85}Cd_{0.15}S$; (d) $Zn_{0.47}Cd_{0.73}$.

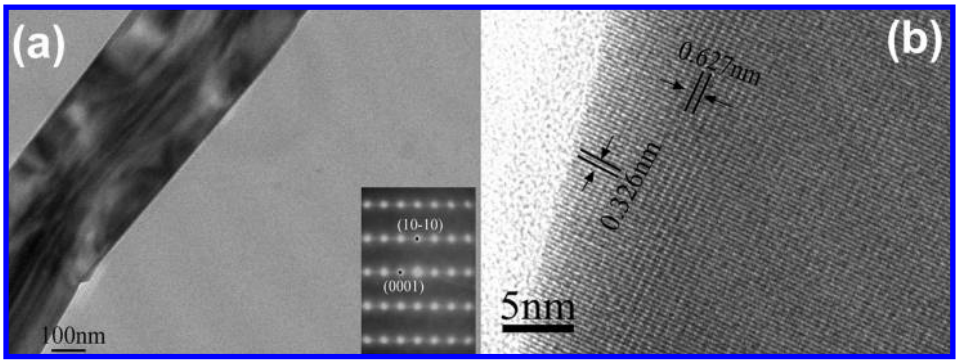

Figure 5. (a) TEM and SAED images and (b) HRTEM image of a ZnS nanoribbon.

nanoribbons with or without sawlike edges are with similar crystallinity.

Shown in images a and b in Figure 6 are the TEM bright-field images and SAED patterns of a single $Zn_{0.85}Cd_{0.15}S$ nanobelt that is ca. 450 nm in width and ca. 80 nm in thickness. One can see "teeth" along the two sides of the nanobelt, and the teeth are about 120 nm in length. SAED patterns in the insets of a and b in Figure 6 suggest single crystallinity and the spots can be indexed to a wurtzite structure with lattice parameters $a = 3.89$ Å and $c = 6.38$ Å. HRTEM images c and d in in Figure 6 further confirm the single crystallinity of the nanobelt, exhibiting 3.35 Å and 6.38 Å lattice spacing of the $(10\bar{1}0)$ and (0001) planes, respectively. The SAED and HRTEM results show that the $Zn_xCd_{1-x}S$ nanobelt grows along the $\langle 10\bar{1}0\rangle$ direction, whereas the teeth along the $\langle 0001\rangle$ direction. The EDX results (not shown) show that element composition at the teeth is similar to that on the surface of the nanobelt, confirming the high homogeneity of the $Zn_xCd_{1-x}S$ solid solutions.

Shown in Figure 7 is a sketch of the ZnS nanoribbon and $Zn_xCd_{1-x}S$ nanobelt. The two nanostructures grow along the $\langle 10\bar{1}0\rangle$ direction, both showing top and bottom surfaces of $(10\bar{1}0)$ orientation and side surfaces of (0001) orientation. The similarities in growth direction and surface orientations are a direct result of the ZnS nanoribbon being used as a template for the synthesis of the $Zn_xCd_{1-x}S$ nanobelt. The related reaction is plausibly: $xZnS + (1 - x)\,CdS \rightarrow Zn_xCd_{1-x}S$. As far as the growth direction of ZnS is concerned, either $\langle 0001\rangle$ or $\langle 10\bar{1}0\rangle$ can be possible. Under suitable conditions or when a vapor−liquid−solid (VLS) mechanism becomes effective, the $\langle 10\bar{1}0\rangle$ direction is possibly a preferred one. It has been reported that the 1D ZnS nanostructures growing on a Au film usually have $\langle 10\bar{1}0\rangle$ growth orientation, showing (0001) and $(10\bar{1}0)$ planes as enclosing facets.[13,14,16,20,21] Accordingly, the $Zn_xCd_{1-x}S$ nanobelts prepared from the ZnS templates have a hexagonal wurtzite phase structure and show $\langle 10\bar{1}0\rangle$ growth orientation.

Figure 8 shows the room-temperature photoluminescence (PL) spectra (using 325 nm laser) of $Zn_xCd_{1-x}S$ nanobelts with different Zn compositions. One can see 352, 368, 383, 396, and 443 nm emissions at $x = 0.94$, 0.85, 0.77, 0.70 and 0.47, respectively. It is clear that by controlling the Zn content of $Zn_xCd_{1-x}S$, one can continuously change the position of the near-bandgap peak from 340 nm (pure ZnS) to 515 nm (pure CdS). The inset of

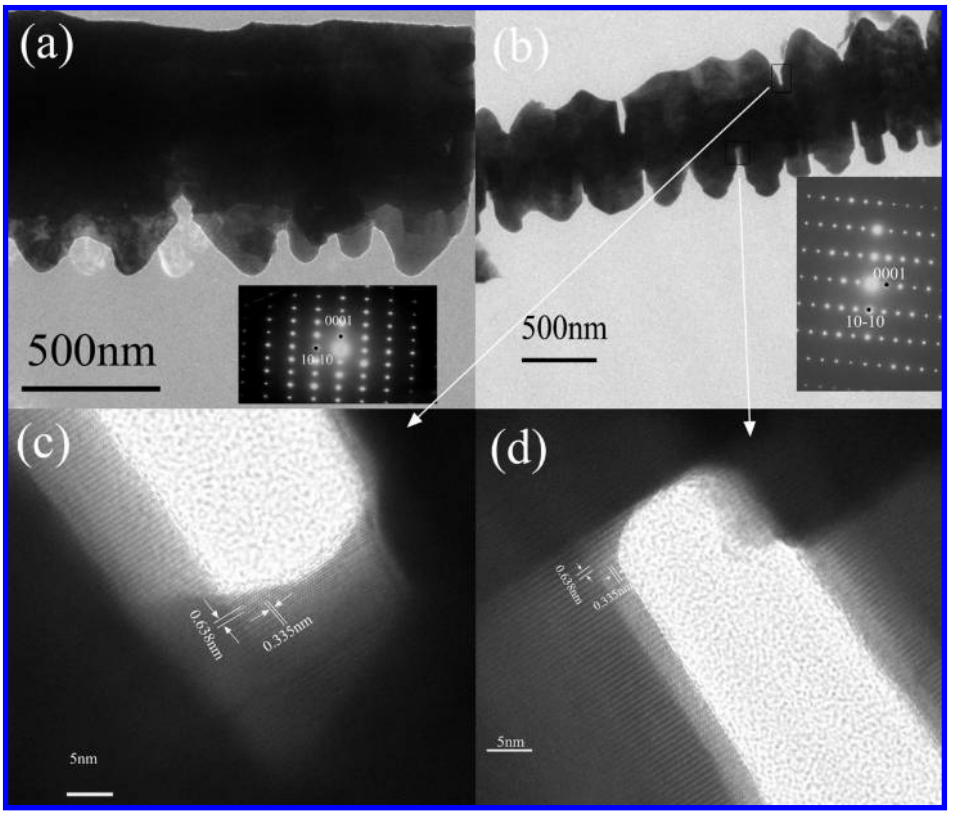

Figure 6. (a) TEM and SAED images of one edge of a $Zn_{0.85}Cd_{0.15}S$ nanobelt, and (b) TEM and SAED images of a $Zn_{0.85}Cd_{0.15}S$ nanobelt showing both sides of the nanobelt; (c) and (d) HRTEM images of the edges of $Zn_{0.85}Cd_{0.15}S$.

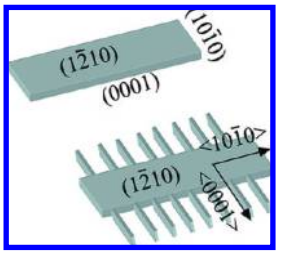

Figure 7. Sketches of a ZnS nanoribbon and a $Zn_xCd_{1-x}S$ nanobelt.

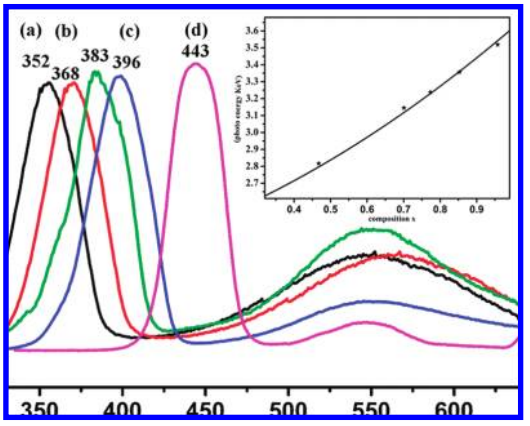

Figure 8. Room-temperature PL spectra of $Zn_xCd_{1-x}S$ nanobelts.

Figure 8 is a plot of the position of the PL peaks as a function of x (obtained based on XRD results). The energy gaps of $Zn_xCd_{1-x}S$: 2.80 (x = 0.47), 3.13 (x = 0.70), 3.24 (x = 0.77), 3.37 (x = 0.85), and 3.52 eV (x = 0.94) are calculated from the PL peaks. For most thin films of II−VI $A_xB_{1-x}C$ semiconductors, the nonlinear variation of energy gaps can be represented as a function of composition: $(E_g(x) = E_{BC} + (E_{AC} - E_{BC} - b)X + bX^2$, where $E_g(x)$ is the energy gap of $A_xB_{1-x}C$; E_{AC} and E_{BC} are the energy gaps of the ending AC and BC members, respectively; and b is a bowing parameter.)[22] As far as a $Zn_xCd_{1-x}S$ film is concerned, the variation in energy gap can be represented as a function of composition ($E_g(x) = 2.337 + 0.72X + 0.563X^2$). As expected, the near-bandgap emission of $Zn_xCd_{1-x}S$ nanobelts is in good agreement with the bandgap values.[19,23] The broad PL peak at about 550 nm is attributable to original deep-trap emission.[24,25] As shown in Figure 9, after 3 h annealing at 600 °C, a $Zn_{0.70}Cd_{0.30}S$ sample is enhanced in crystallinity, showing band-edge PL peak that is narrower, more symmetric, and stronger than that of the nonannealed one. It is clear that the annealing step can eliminate defects and stresses inside the crystal

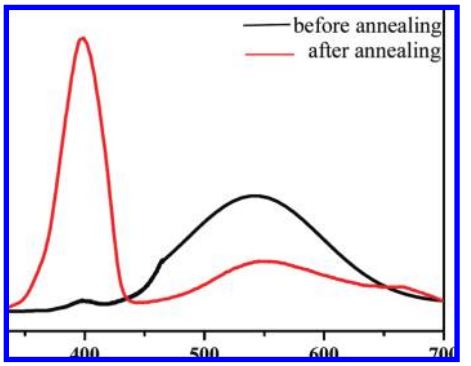

Figure 9. PL spectra of $Zn_{0.70}Cd_{0.30}S$ nanobelts before and after annealing.

lattice, and with the removal of defects, there is decrease in deep-trap emission. Such properties of the materials make the two-step thermal evaporation method reproducible and controllable for the fabrication of $Zn_xCd_{1-x}S$ nanobelts for a specified emission. It is envisaged that the same approach can be adopted to fabricate $Zn_xCd_{1-x}S$ quantum dots of specific PL emissions, similar to those reported by Zhong et al.[25] By chemical methods at low temperature, Zhong et al. prepared alloyed $Zn_xCd_{1-x}S$ quantum dots that show random spatial composition fluctuations. After high-temperature annealing, high-quality alloyed $Zn_xCd_{1-x}S$ nanocrystallites with composition homogeneity were formed. Despite different in morphology and dimension, the nanobelts and quantum dots of $Zn_xCd_{1-x}S$ can be improved in quality by annealing for narrow and strong near-bandgap emission as well as for deep-trap emission suppression. Because the $Zn_xCd_{1-x}S$ nanobelts are produced at high temperatures by physical method (two-step evaporation), the quality of the nonannealed crystals is mainly affected by the defects and stresses inside the crystal lattice rather than by factor such as random spatial composition fluctuations. The annealing process can eliminate defects and stresses but has little to do with the alteration of spatial composition.

In summary, through a method of two-step evaporation, we have synthesized $Zn_xCd_{1-x}S$ nanobelts of specific near-band PL emissions in a controllable manner. By means of proper annealing, the crystallinity of $Zn_xCd_{1-x}S$ can be enhanced for better near-band emission (strong and narrow). The nanobelts of $Zn_xCd_{1-x}S$ solid solutions are ideal nanoemitters potentially applicable as light-emitting devices or semiconductor lasers in optoelectronic applications. The fabrication of $Zn_xCd_{1-x}S$ is based on the use of ZnS nanoribbons as template. We envisage that the simple method can be extended to synthesizing nanostructures of other materials.

Acknowledgment. This work was supported by the National Natural Science Foundation of China (Grant 10674059), the National High Technology Research and Development Program of China (Grant 2007AA021805), and the National Key Project for Basic Research (Grant 2005CB623605 and 2010CB923402), People's Republic of China.

References

(1) Pan, Z. W.; Dai, Z. R.; Wang, Z. L. *Science* **2001**, *291*, 1947.
(2) Xia, Y. N.; Yang, P. D.; Sun, Y. G.; Wu, Y. Y.; Mayers, B.; Gates, B.; Yin, Y.; Kim, F.; Yan, H. *Adv. Mater.* **2003**, *15*, 353.
(3) (a) Morales, A. M.; Lieber, C. M. *Science* **1998**, *279*, 208. (b) Huang, Y.; Duan, X.; Cui, Y.; Lauhon, L.; Kim, K.; Lieber, C. M. *Science* **2001**, *194*, 1919. (c) Lieber, C. M.; Wang, Z. L. *MRS Bull.* **2007**, *32*, 99. (d) Tian, B.; Kempa, T. J. *Chem. Soc. Rev.* **2009**, *38*, 16.
(4) Iijima, S. *Nature* **1991**, *354*, 56.
(5) Pal, S.; Goswami, B.; Sarkar, P. *J. Phy. Chem. C* **2007**, *111*, 1557.
(6) (a) Subramoney, S. *Adv. Mater.* **1998**, *10*, 1157. (b) Aleshin, N. A. *Adv. Mater.* **2006**, *18*, 17.
(7) Fang, X. S.; Zhang, L. D. *J. Mater. Sci. Technol.* **2006**, *22*, 1.
(8) Zhu, Y. C.; Bando, Y. S.; Xue, D. F. *Appl. Phy. Lett.* **2003**, *82*, 1769.
(9) Xu, X. J.; Fei, G. T.; Yu, W. H.; Wang, X. W.; Chen, L.; Zhang, L. D. *Nanotechnology* **2006**, *17*, 426.
(10) Jing, Y.; Meng, X. M.; Liu, J.; Hong, Z. R.; Lee, C. S.; Lee, S. T. *Adv. Mater.* **2003**, *15*, 1195.
(11) (a) Shen, G. Z.; Bando, Y.; Hu, J. Q.; Golberg, D. *Appl. Phy. Lett.* **2007**, *90*, 123101. (b) Sun, H. Y.; Li, X. H.; Li, W.; Li, F.; Liu, B. T.; Zhang, X. Y. *Nanotechnology* **2007**, *18*, 115604.
(12) Lee, J. H.; Song, W. C.; Yi, J. S.; Yang, K. J.; Han, W. D.; wang, J. H. *Thin Solid Films* **2003**, *431 −432*, 349.
(13) (a) Li, Y. J.; You, L. P.; Duan, R.; Shi, P. B.; Du, H. L.; Qiao, Y. P.; Qin, G. G. *Nanotechnology* **2004**, 581. (b) Yao, W. T.; Yu, S. H.; Pan, L.; Li, J.; Wu, Q. S.; Zhang, L.; Jiang, J. *small* **2005**, *1*, 320.
(14) (a) Fang, X. S.; Bando, Y.; Ye, C. H.; Golberg, D. *Chem. Commun.* **2007**, 3048. (b) Fang, X. S.; Gautam, U. K.; Bando, Y.; Golberg, D. *J. Mater. Sci. Technol.* **2008**, *24*, 520.
(15) (a) Moore, D.; Wang, Z. L. *J. Mater. Chem.* **2006**, *16*, 3898. (b) Moore, D.; Ding, Y.; Wang, Z. L. *J. Am. Chem. Soc.* **2004**, *126*, 14372.
(16) (a) Fang, X. S.; Bando, Y.; Shen, G. Z.; Ye, C. H.; Gautam, U. K.; Costa, P. M. F. J.; Zhi, C. Y.; Tang, C. C.; Golberg, D. *Adv. Mater.* **2007**, *19*, 2593. (b) Fang, X. S.; Bando, Y.; Liao, M. Y.; Gautam, U. K.; Zhi, C. Y.; Dierre, B. J.; Liu, B. D.; Zhai, T. Y.; Sekiguchi, T.; Koide, Y.; Golberg, D. *Adv. Mater.* **2009**, *21*, 2034.
(17) (a) Ballentyne, D. W. G.; Ray, B. *Physica* **1961**, *27*, 337. (b) Denton, A. R.; Ashchroft, N. W. *Phys. Rev. A* **1991**, *43*, 3161.
(18) shimaoka, G.; Suzuki, Y. *Appl. Phys. Sci.* **1997**, *113*, 528.
(19) Liu, Y. K.; Zapien, J. A.; Shan, Y. Y.; Geng, C. Y.; Lee, C. S.; Lee, S. T. *Adv. Mater.* **2005**, *17*, 1372.
(20) Hao, Y. F.; Meng, G. W.; Wang, Z. L.; Ye, C. H.; Zhang, L. D. *Nano Lett.* **2006**, *6*, 1650.
(21) Borchers, C.; Stichtenoth, D.; Muller, S.; Schwen, D.; Ronning, C. *Nanotechnology* **2006**, *17*, 1067.
(22) (a) Hill, R. *J. Phys. C: Solid State Phys.* **1974**, *7*, 521. (b) Richardson, D.; Hill, R. *J. Phys. C: Solid State Phys.* **1972**, *5*, 821. (c) Venugopal, R.; Lin, P. I.; Chen, Y. S. *J. Phys. Chem. B* **2006**, *110*, 11691.
(23) Salem, A. M. *Appl. Phys. A: Mater. Sci. Process* **2002**, *74*, 205.
(24) Ouyang, J. Y.; Ratcliffe, C. I.; Kingston, D.; Wilkinson, B.; Kuijper, J.; Ripmeester, J. A.; Yu, K. *J. Phys. Chem. C* **2008**, *112*, 4908.
(25) Zhong, X. H.; Feng, Y. Y.; Knoll, W. G.; Han, M. Y. *J. Am. Chem. Soc.* **2003**, *125*, 13559.